Electronic Supplementary Information (ESI)

Role of reaction intermediate diffusion on the performance of platinum electrodes in solid acid fuel cells

Oliver Lorenz[1*,†], Alexander Kühne[1†], Martin Rudolph[1], Wahyu Diyatmika[1], Andrea Prager[1], Jürgen W. Gerlach[1], Jan Griebel[1], Sara Winkler[2], Andriy Lotnyk[1], André Anders[1,3] and Bernd Abel[1,2]

[1] Leibniz Institute of Surface Engineering (IOM), Permoserstraße 15, 04318 Leipzig, Germany
[2] Ostwald-Institute of Physical and Theoretical Chemistry, Department of Chemistry and Mineralogy, Leipzig University, Linnéstraße 3, 04103 Leipzig, Germany
[3] Felix Bloch Institute of Solid State Physics, Faculty of Physics and Earth Science, Leipzig University, Linnéstraße 5, 04103 Leipzig, Germany
* Correspondence: oliver.lorenz@iom-leipzig.de; Tel.: +49 341 235 4029

† Both authors contributed equally

ESI1: Grain size measurement from the scanning electron micrographs

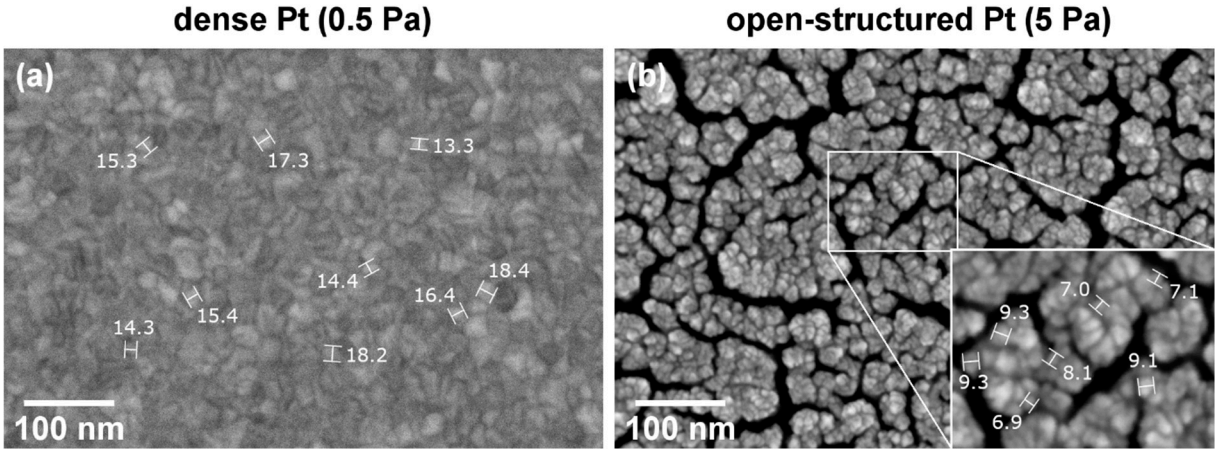

Figure S1: Representative scanning electron micrographs of the 60 nm thick dense (left hand side) and open-structured (right hand side; including an enlarged insertion) Pt thin film deposited onto a Si substrate. The representative measured grain size (in nm) are marked white brackets.

ESI2: Scanning electron micrographs of the microporous layer on the carbon paper

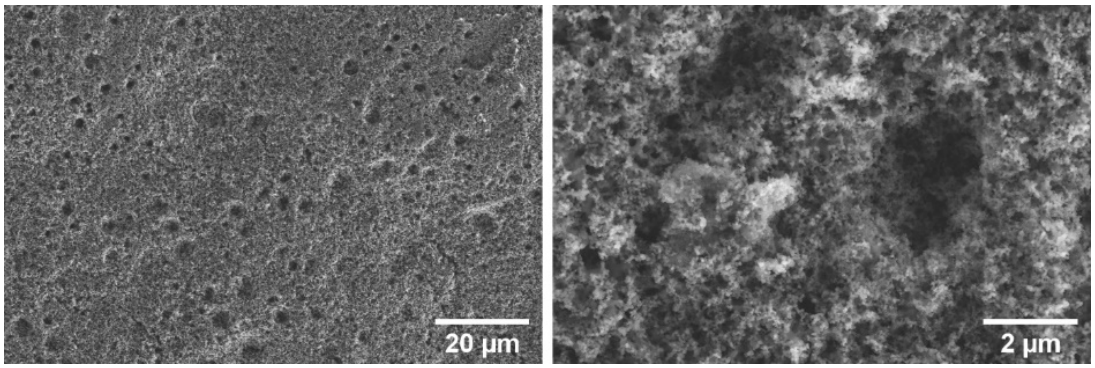

Figure S2: Representative scanning electron micrographs of the Freudenberg carbon paper including a microporous layer.

ESI3: Staircase potential electrochemical impedance spectroscopy from 250 mV up to 550 mV

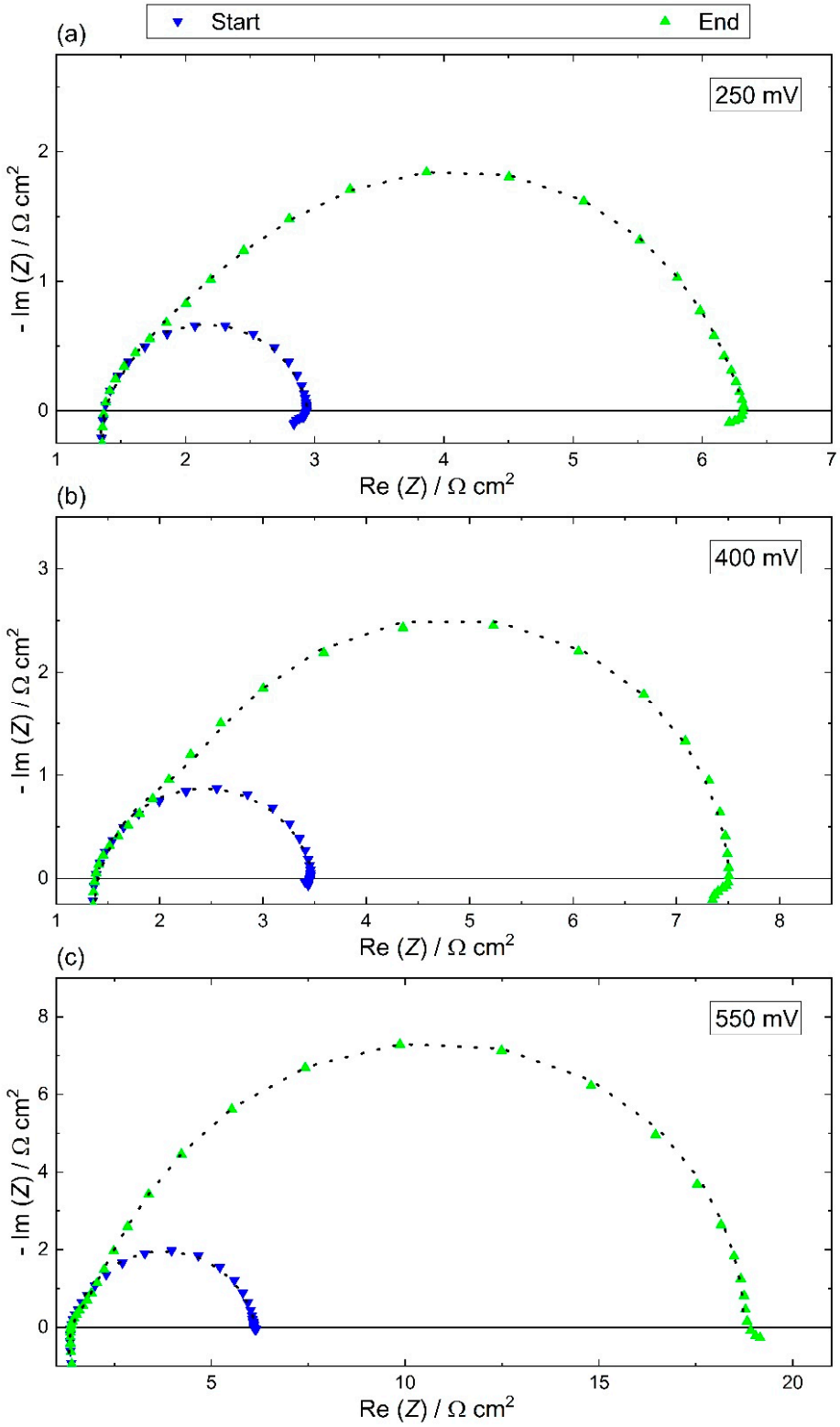

Figure S3: Staircase potential impedance spectroscopy from 250 up to 550 mV vs. pseudo-hydrogen electrode pre and post fuel cell operation (60 h @ 60 mA cm^{-2}, 0.3 atm H_2O, 30 sccm H_2, 30 sccm O_2). The black dotted lines representing the fits for the equivalent circuits' models consisting of a series of inductor and ohmic resistance, and

in parallel a constant-phase element (CPE) with an ohmic resistance (Start) and the RCDP subcircuit was extended with finite-length Warburg diffusion element (End).

ESI4: Representative Micrographs 15 h post fuel cell operation

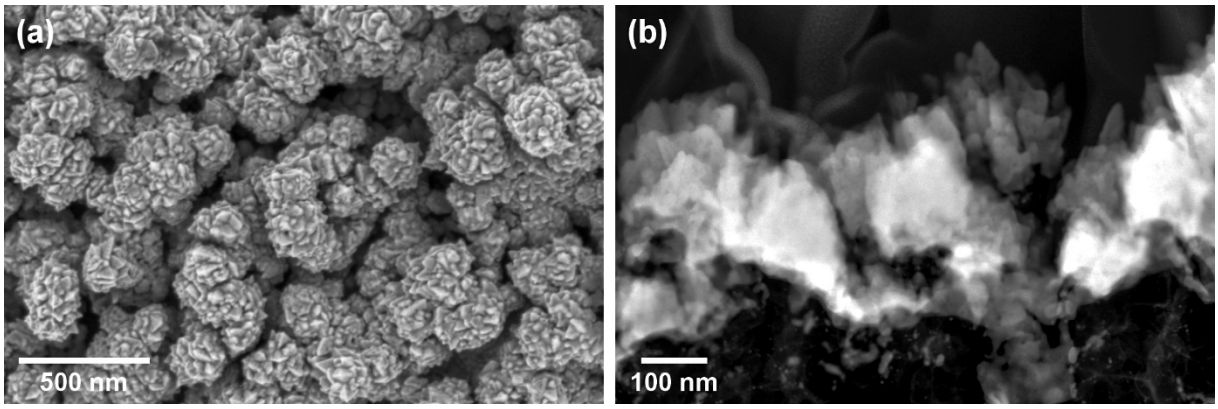

Figure S4: Representative scanning (a) and scanning (b) transmission electron micrographs post 15 h of fuel cell operation.

ESI5: *In situ* measurement of the electrochemically active surface (ECSA)

The ECSA measurement was performed according to Lohmann-Richters et al.[4] To date, the platinum oxide reduction peak is the only published approach to determine the ECSA for SAFC. For a comprehensive discussion of other possible methods, we recommend the above-mentioned publication. As the upper vertex potential increases, the fuel cell performance decreases (see Figure S5).

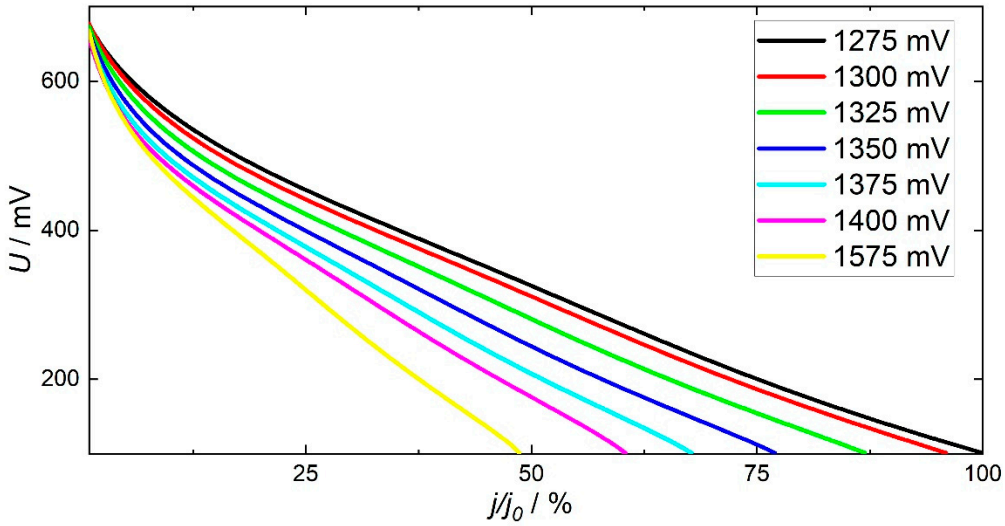

Figure S5: The polarization curves of fuel cell during the ECSA measurement. The current density depends on the upper vertex potential. The upper vertex potential is marked in the legend. The current density j is normalized to the initial current density j_0 at 100 mV vs. pseudo-hydrogen electrode.

During the ECSA measurement, the electrode performance changes and thus the measurement does not reflect the initial ECSA due to the power drop. We assume that the fuel cell performance decay must be linked to a potential induced carbon corrosion.[5]

ESI6: Representative Pt layer thickness measurement of the deposited thin films

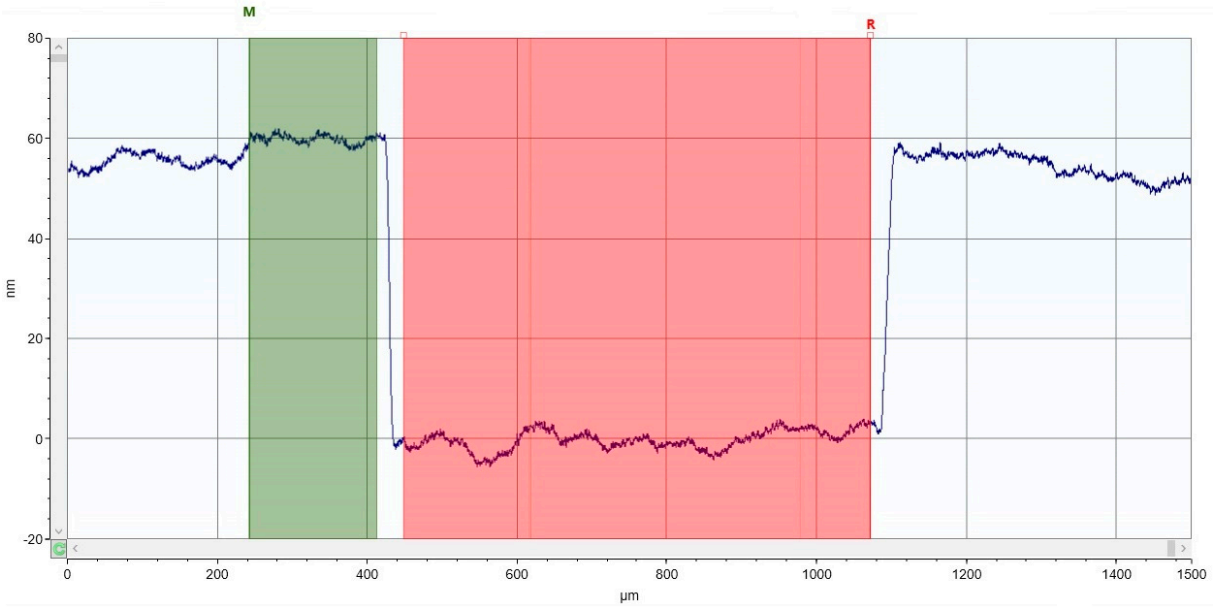

Figure S6: Representative tactile profilometry measurement of the platinum layer thickness. The step height between the Si surface (marked in red) and the film surface (marked in green) reveals the layer thickness of 60 nm.

ESI7: Powder X-ray diffraction pattern of the synthesized electrolyte particles

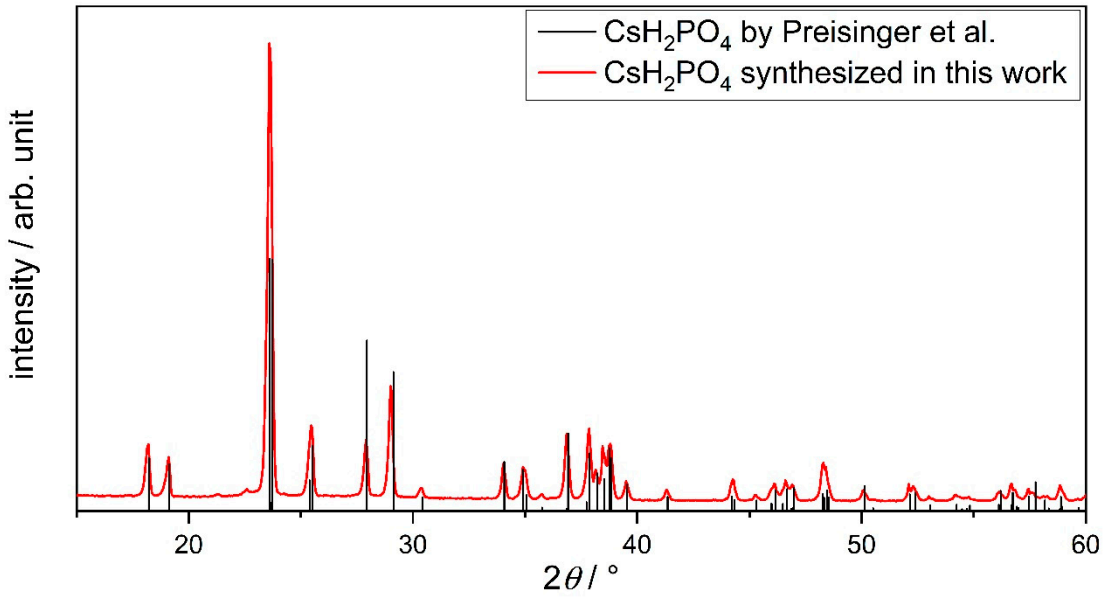

Figure S7: X-ray diffraction pattern (using Cu Kα) of the synthesized electrolyte CsH_2PO_4 powder in this work and the powder data published by Preisinger et al.[1] (with offset for better presentation). The diffraction data from Preisinger were obtained from the Cambridge Structural Database (CCDC number 1639853) and the presented diffraction pattern was predicted using the software PLATON.

ESI8: Pt film growth onto lapped Si and glass substrate

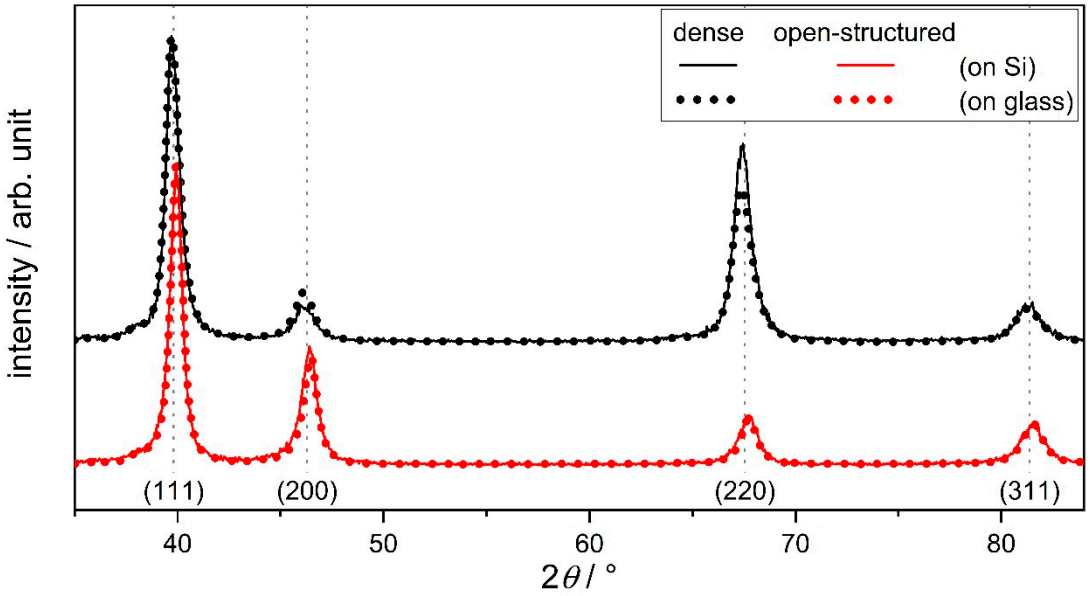

Figure S8: Grazing incidence X-ray diffraction patterns (using Cu Kα) of the 60 nm thick dense and open-structured Pt thin films deposited on Si wafer and glass substrate (intensity normalized to Pt{111}, y-axis offset for better presentability). Reference positions of the X-ray reflections based on Davey et al.[2]

To investigate a possible substrate-induced growth effect, the films were deposited onto amorphous glass and lapped monocrystalline Si substrate. Since there are strong differences of the substrate crystallinity and roughness a preferred orientation should be influenced by this. The grazing incidence X-ray diffraction (GID) patterns reveals a larger intensity difference between the I_{200}/I_{111} in the dense and the open-structured case compared to the pattern of the films on carbon paper (Figure S3). However, the same trend for dense and open-structured case on each substrate is notable. Note that the GID patterns on Si and glass substrates show the same behavior for the open-structured film and small differences for the dense film. In addition, with the comparison of the SEM micrographs, it can be argued that insights from the microstructural analysis of the Pt thin films on Si substrates are valid for the prepared GDEs.

ESI9: Grain size determination based on the X-ray diffraction patterns

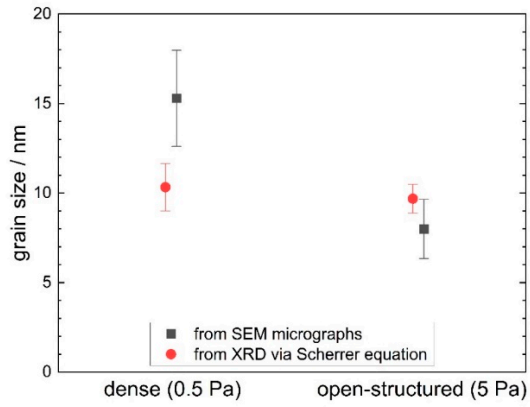

Figure S9: Comparison between the grain sizes estimated from XRD patterns via Scherrer equation (Figure S3) and measured by the SEM micrographs.

The grain domain size estimated via the Scherrer equation are almost equal for dense and open-structured Pt thin film with a slightly higher value for the dense film. For the open-structured film, the grain domain sizes from the Scherrer equation correlates well with SEM measurements whereas the grain sizes for the dense films differ. Since there are no information about additional peak broadening effects like crystallite shapes and distribution or other instrumental and non-instrumental factors, this Scherrer equation can only be used as good approximation. [3] However, for evaluation of the catalytic performance it is important to focus on the information provided by the surface morphology measurements and notice the slightly bigger grains for the dense Pt film as seen in the scanning electron micrographs.

ESI10: Residuals obtained from the linear Kramers-Kronig test

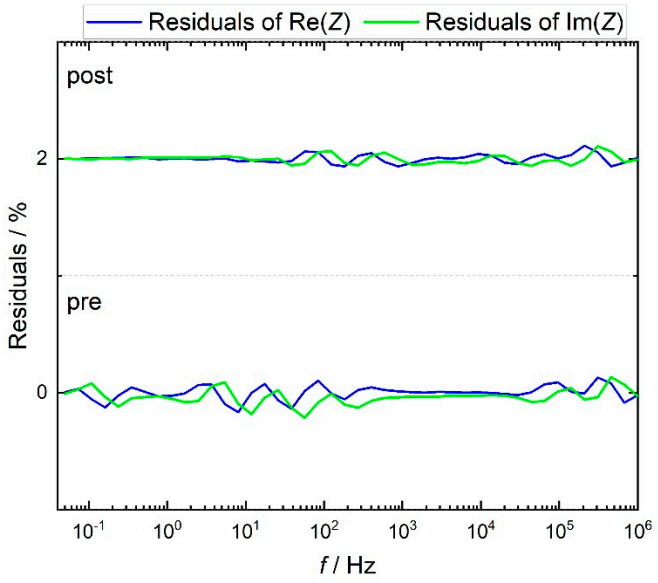

Figure S10a: Impedance data residuals (blue- residuals of Re(Z) and green- residuals of Im(Z)) from the potential electrochemical impedance measurement pre and post fuel cell operation (with an offset of 2%) according to the Kramers-Kronig relation. The dotted, grey lines present the validity region of ±1%.

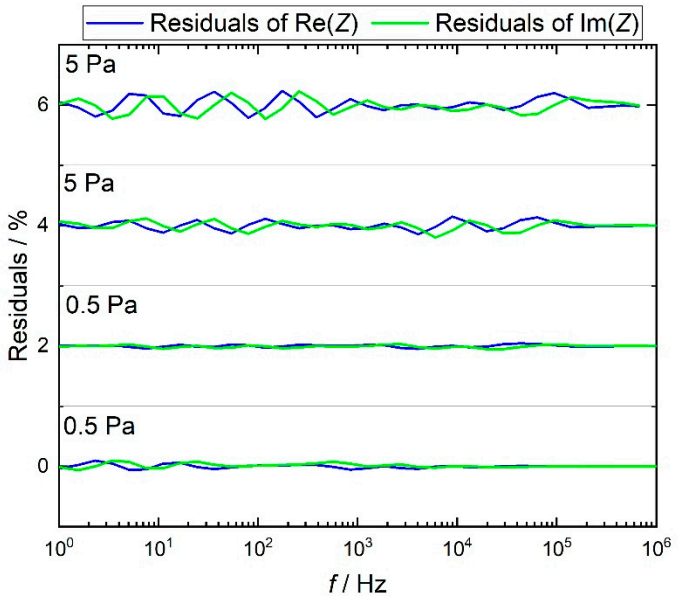

Figure S10b: Impedance data residuals (blue- residuals of Re(Z) and green- residuals of Im(Z)) from the impedance measurement under anodic conditions for two 0.5 and 5 Pa MEAs according to the Kramers-Kronig relation. For clarification, each measurement has an offset of 2%. The dotted, grey lines present the validity region of ±1%.

ESI11: Nyquist representation of the open-structured gas diffusion electrode impedance with varied layer thicknesses

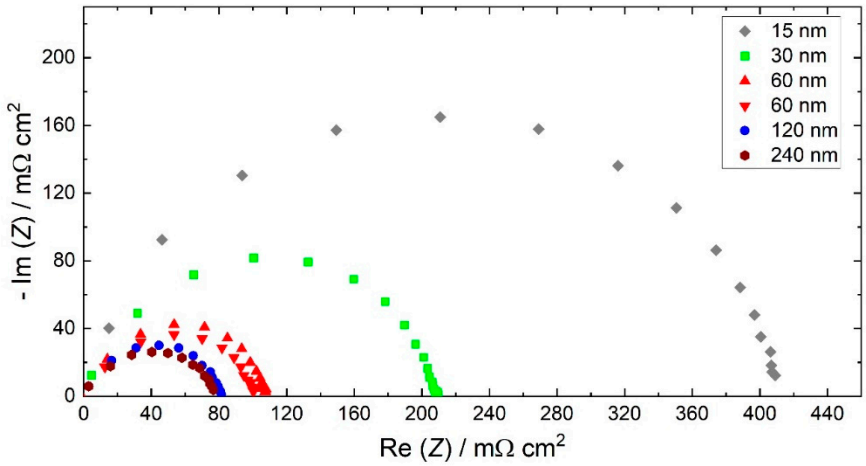

Figure S11: Nyquist representation of the open-structured GDE impedance of the varied layer thicknesses measured under anodic fuel cell conditions (513 K, 60 sccm H_2 and 0.3 atm H_2O).

References

(1) Preisinger, A.; Mereiter, K.; Bronowska, W. The Phase Transition of CsH_2PO_4 (CDP) at 505 K. *Materials Science Forum* **1994**, *166–169*, 511–516. https://doi.org/10.4028/www.scientific.net/MSF.166-169.511.

(2) Davey, W. P. Precision Measurements of the Lattice Constants of Twelve Common Metals. *Phys. Rev.* **1925**, *25* (6), 753–761. https://doi.org/10.1103/PhysRev.25.753.

(3) Holzwarth, U.; Gibson, N. The Scherrer Equation versus the "Debye-Scherrer Equation." *Nature Nanotech* **2011**, *6* (9), 534–534. https://doi.org/10.1038/nnano.2011.145.

(4) Lohmann-Richters, F. P.; Abel, B.; Varga, Á. In Situ Determination of the Electrochemically Active Platinum Surface Area: Key to Improvement of Solid Acid Fuel Cells. *Journal of Materials Chemistry A* **2018**, *6* (6), 2700–2707. https://doi.org/10.1039/C7TA10110D.

(5) Macauley, N.; Papadias, D. D.; Fairweather, J.; Spernjak, D.; Langlois, D.; Ahluwalia, R.; More, K. L.; Mukundan, R.; Borup, R. L. Carbon Corrosion in PEM Fuel Cells and the Development of Accelerated Stress Tests. *J. Electrochem. Soc.* **2018**, *165* (6), F3148–F3160. https://doi.org/10.1149/2.0061806jes.